



Please cite this article in press as: Minekawa A, et al., Cochlear outer hair cells in a dominant-negative connexin26 mutant mouse preserve non-linear capacitance in spite of impaired distortion product otoacoustic emission, *Neuroscience* (2009), doi: 10.1016/j.neuroscience.2009.08.043

*Neuroscience* xx (2009) xxx

## COCHLEAR OUTER HAIR CELLS IN A DOMINANT-NEGATIVE CONNEXIN26 MUTANT MOUSE PRESERVE NON-LINEAR CAPACITANCE IN SPITE OF IMPAIRED DISTORTION PRODUCT OTOACOUSTIC EMISSION

A. MINEKAWA,<sup>a</sup> T. ABE,<sup>b</sup> A. INOSHITA,<sup>a</sup> T. IIZUKA,<sup>a</sup> S. KAKEHATA,<sup>b</sup> Y. NARUI,<sup>a</sup> T. KOIKE,<sup>c</sup> K. KAMIYA,<sup>a</sup> H.-O. OKAMURA,<sup>c</sup> H. SHINKAWA<sup>b</sup> AND K. IKEDA<sup>a\*</sup>

<sup>a</sup>Department of Otorhinolaryngology, Juntendo University School of Medicine, Tokyo, Japan

<sup>b</sup>Department of Otorhinolaryngology, Hirosaki University School of Medicine, Hirosaki, Japan

<sup>c</sup>Department of Mechanical Engineering and Intelligent Systems, The University of Electro-Communications, Tokyo, Japan

**Abstract**—Mutations in the connexin26 gene (*GJB2*) are the most common genetic cause of congenital bilateral non-syndromic sensorineural hearing loss. Transgenic mice were established carrying human Cx26 with the R75W mutation that was identified in a deaf family with autosomal dominant negative inheritance [Kudo T et al. (2003) *Hum Mol Genet* 12:995–1004]. A dominant-negative *Gjb2* R75W transgenic mouse model shows incomplete development of the cochlear supporting cells, resulting in profound deafness from birth [Inoshita A et al. (2008) *Neuroscience* 156:1039–1047]. The Cx26 defect in the *Gjb2* R75W transgenic mouse is restricted to the supporting cells; it is unclear why the auditory response is severely disturbed in spite of the presence of outer hair cells (OHCs). The present study was designed to evaluate developmental changes in the *in vivo* and *in vitro* function of the OHC, and the fine structure of the OHC and adjacent supporting cells in the R75W transgenic mouse. No detectable distortion product otoacoustic emissions were observed at any frequencies in R75W transgenic mice throughout development. A characteristic phenotype observed in these mice was the absence of the tunnel of Corti, Nuel's space, and spaces surrounding the OHC; the OHC were compressed and squeezed by the surrounding supporting cells. On the other hand, the OHC developed normally. Structural features of the lateral wall, such as the membrane-bound subsurface cisterna beneath the plasma membrane, were intact. Prestin, the voltage-dependent motor protein, was observed by immunohistochemistry in the OHC basolateral membranes of both transgenic and non-transgenic mice. No significant differences in electromotility of isolated OHCs during development was observed between transgenic and control mice. The present study indicates that normal development of the supporting cells is indispensable for proper cellular function of the OHC. © 2009 IBRO. Published by Elsevier Ltd. All rights reserved.

**Key words:** hereditary deafness, connexin26, *Gjb2*, outer hair cell, prestin, electromotility.

\*Corresponding author. Tel: +81-3-5802-1229; fax: +81-3-5840-7103. E-mail address: ike@juntendo.ac.jp (K. Ikeda).

**Abbreviations:** C<sub>m</sub>, membrane capacitance; C<sub>n</sub>, nonlinear capacitance; Cx26, connexin26; DAPI, 4',6-diamidino-2-phenylindole; DPOAE, distortion product otoacoustic emission; *GJB2*, connexin26 gene; OHC, outer hair cell; P, postnatal day; PB, phosphate buffer; PBS, phosphate-buffered saline; PFA, paraformaldehyde.

0306-4522/09 \$ - see front matter © 2009 IBRO. Published by Elsevier Ltd. All rights reserved.  
doi:10.1016/j.neuroscience.2009.08.043

The organ of Corti in mammals is a complex three-dimensional structure containing both sensory and supporting cells sitting on the basilar membrane. The supporting cells, including the pillar cells and Deiter's cells, form a rigid scaffold adjacent to and surrounding the outer hair cell (OHC) and confer essential mechanical properties for efficient transmission of stimulus-induced motion of the hair cells between the reticular lamina and the basilar membrane. Although development of pillar cells and the formation of a normal tunnel of Corti are required for normal hearing (Colvin et al., 1996), the physiological function of the supporting cells in postnatal development remains unclear.

Gap junction proteins in the cochlear supporting cells are believed to allow rapid removal of K<sup>+</sup> away from the base of hair cells, resulting in recycling back to the endolymph (Kikuchi et al., 1995). In addition to these effects on K<sup>+</sup>, gap junction proteins act to mediate Ca<sup>2+</sup> and anions such as inositol 1,4,5-trisphosphate, ATP, and cAMP as cell-signaling, nutrient, and energy molecules (Beltramello et al., 2005; Zhao et al., 2005; Piazza et al., 2007; Gossman and Zhao, 2008). In the developing postnatal cochlea, Tritsch et al. (2007) further found that within a transient structure known as Kolliker's organ, ATP can bind to P2X receptors on the inner hair cells, thus causing depolarization and Ca<sup>2+</sup> influx, while also mimicking the effect of sound.

In the organ of Corti, most gap junctions are assembled from connexin (Cx) protein subunits, predominantly connexin 26 (Cx26, *Gjb2* gene) and co-localized Cx30 (Forge et al., 2003; Zhao and Yu, 2006). Mouse models have confirmed that Cx26 encoded by *Gjb2* is essential for cochlear function (Cohen-Salmon et al., 2002; Kudo et al., 2003). A dominant-negative *Gjb2* R75W transgenic mouse model shows incomplete development of the cochlear supporting cells, resulting in profound deafness from birth (Inoshita et al., 2008). Characteristic ultrastructural changes observed in the developing supporting cells of the *Gjb2* R75W transgenic mouse model include (i) the absence of the tunnel of Corti, Nuel's space, or spaces surrounding the OHCs; and (ii) reduced numbers of microtubules in the pillar cells. On the other hand, the development of the OHCs, at least from postnatal day 5 (P5) to P12 was not affected. The Cx26 defect in the *Gjb2* transgenic mouse is restricted to the supporting cells; it is thus difficult to explain why the auditory response is extensively disturbed despite the presence of the OHCs.

The present study was designed to evaluate developmental changes in the *in vivo* and *in vitro* function of the OHC together with the ultrastructure of the OHC and its adjacent

supporting cells in the R75W transgenic mouse, to provide a better understanding of the functional properties of the supporting cells, and to gain new insights into the molecular and physiological mechanisms of *Gjb2*-based deafness.

## EXPERIMENTAL PROCEDURES

### Animals and anesthesia

All mice used for this study were obtained from a breeding colony of R75W transgenic mice (Kudo et al., 2003) and maintained at the Institute for Animal Reproduction (Ibaraki, Japan). R75W transgenic mice were maintained on a mixed C57BL/6 background and intercrossed to generate R75W transgenic animals. The animals were genotyped using DNA obtained from tail clips and amplified with the Tissue PCR Kit (Sigma, Saint Louis, MO, USA). The animals were deeply anesthetized with an intraperitoneal injection of ketamine (100 mg/kg, Ohara Pharmaceutical Co., Ltd., Tokyo, Japan) and xylazine (10 mg/kg) in all experiments. All experiment protocols were approved by the Institutional Animal Care and Use Committee at Juntendo University School of Medicine, and were conducted in accordance with the US National Institutes of Health Guidelines for the Care and Use of Laboratory Animals.

### Distortion product otoacoustic emission

All electrophysiology was performed within an acoustically and electrically insulated and grounded test room. Distortion product otoacoustic emission (DPOAE) responses at 2f<sub>1</sub>-f<sub>2</sub> were measured through the meatus using a measuring system (model ER-10B, Etymotic Research Inc., Elk Grove Village, IL, USA) with a probe developed for immature mice according to a previous paper (Narui et al., 2009). DPOAE stimuli were administered at two primary frequencies, f<sub>1</sub> and f<sub>2</sub>, such that f<sub>1</sub><f<sub>2</sub>. DPOAE input/output functions at f<sub>2</sub>=12, 30, and 45 kHz with f<sub>2</sub>/f<sub>1</sub>=1.2 were constructed. At each frequency pair, primary levels L1 (level of f<sub>1</sub> tone) and L2 (level of f<sub>2</sub> tone) were increased incrementally by 5 dB steps from 30 to 80 dB (f<sub>2</sub>=12 kHz and 30 kHz), and 30 to 70 dB (f<sub>2</sub>=45 kHz) with L<sub>1</sub>=L<sub>2</sub>. The DPOAE threshold level was defined as the dB level at which the 2f<sub>1</sub>-f<sub>2</sub> distortion product was more than 10 dB above the noise level.

### Non-linear capacitance

OHCs were obtained from acutely dissected organs of Corti from both transgenic and non-transgenic mice according to a previous report (Abe et al., 2007). Briefly, cochleae were dissected, and the organs of Corti were separated from the modiolus and stria vascularis. The organs were then digested with trypsin (1 mg/ml) in external solution (100 mM NaCl, 20 mM tetraethylammonium, 20 mM CsCl, 2 mM CoCl<sub>2</sub>, 1.52 mM MgCl<sub>2</sub>, 10 mM 4-(2-hydroxyethyl)-1-piperazineethanesulfonic acid and 5 mM dextrose (pH 7.2), 300 mosmol/L, in order to block ionic conductance) for 10–12 min at room temperature and transferred into 35 mm plastic dishes (Falcon, Lincoln Park, NJ, USA) with 2 ml external solution. OHCs were isolated by gentle trituration. The dish was mounted on an inverted microscope (IX71; Olympus, Tokyo, Japan).

The patch pipette solution contained 140 mM CsCl, 2 mM MgCl<sub>2</sub>, 10 mM ethyleneglycoltetraacetic acid, 10 mM 4-(2-hydroxyethyl)-1-piperazineethanesulfonic acid (pH 7.2), 300 mosmol/L (adjusted with dextrose).

The cells were whole-cell voltage-clamped with an Axon (Burlingame, CA, USA) 200 B amplifier using patch pipettes having initial resistances of 3–5 MΩ. Series resistances, which ranged 5–20 MΩ, remained uncompensated for membrane capacitance (C<sub>m</sub>) measurements, though corrections for series resistance voltage errors were made offline.

Data acquisition and analysis were performed using the Windows-based patch-clamp program jClamp (SciSoft, New Haven, CT, USA).

The C<sub>m</sub> functions were obtained 1 min after establishment of the whole-cell configuration. C<sub>m</sub> was assessed using a continuous high-resolution (2.56 ms sampling) two-sine voltage stimulus protocol (10 mV peak at both 390.6 and 781.2 Hz) superimposed onto a voltage ramp (200 ms duration) from -150 to +150 mV (Santos-Sacchi et al., 1998; Santos-Sacchi, 2004). The capacitance data were fit to the first derivative of a two-state Boltzmann function (Santos-Sacchi, 1991).

$$C_m = Q_{\max} \frac{ze}{kT} \frac{b}{(1+b)^2} + C_{lin}$$

$$b = \exp\left(\frac{-ze(V_m - V_{pkcm})}{kT}\right)$$

where Q<sub>max</sub> is the maximum nonlinear charge moved, V<sub>pkcm</sub> is voltage at peak capacitance or half-maximum charge transfer, V<sub>m</sub> is membrane potential, z is valence, C<sub>lin</sub> is linear membrane capacitance, e is electron charge, k is Boltzmann's constant, and T is absolute temperature. For analyses, we quantified C<sub>v</sub>, peak, an estimate of maximum voltage-dependent, nonlinear capacitance, as the absolute peak capacitance minus linear capacitance.

### Histology

The mice were perfused with 4.0% paraformaldehyde (PFA) and 2.0% glutaraldehyde (pH 7.4) in 0.1 M phosphate buffer (PB). The inner ears were dissected and immersed in fixative overnight at room temperature. Decalcification was completed by immersion in 0.12 M ethylenediaminetetraacetic acid with gentle stirring at room temperature for a day. The cochleas were flushed again with buffer prior to perfusion with a warm solution of 10% gelatin. They were chilled on ice, thus allowing the gelatin to solidify, and then cut in half under a dissecting microscope. The half cochleas were rinsed (four times for 1 min each) with warm PB (40 °C) to remove residual gelatin. The specimens were post-fixed 1.5 h in 2.0% OsO<sub>4</sub> in 0.1 M PB, then dehydrated through graded ethanol and embedded in Epon. Semithin sections (1 μm) were stained with Toluidine Blue for light microscopy. Ultrathin sections were stained with uranyl acetate and lead citrate and examined by electron microscopy (HITACHI H7100, Japan).

### Immunohistochemistry

The cochleae were removed after cardiac perfusion with 4% PFA (pH 7.4), placed in the same fixative at room temperature for 1 h, decalcified with 0.12 M ethylenediaminetetraacetic acid (pH 7.0) at 4 °C overnight. The specimens were dehydrated through graded concentrations of alcohol, embedded in paraffin blocks and sectioned into 5 μm thick slices. The sections were washed in several changes of 0.01 M phosphate-buffered saline (PBS; pH 7.2), blocked with 2% bovine serum albumin in 0.01 M PBS for 30 min, and then were incubated for 1 h at room temperature with goat polyclonal antibodies to Prestin (1:100; Santa Cruz Biotechnology, Santa Cruz, CA, USA) (Kitsunai et al., 2007) diluted in 0.01 M PBS+1% bovine serum albumin. The following day, the tissues were rinsed with 0.01 M PBS, incubated for 1 h at room temperature with a Alexa-Fluor-594 conjugated donkey anti-goat (1:1000; Molecular Probes, Eugene, OR, USA), rinsed with 0.01 M PBS, and then mounted in Vectashield containing DAPI (Vector Laboratories, Burlingame, CA, USA). Labeling was viewed using a confocal laser scanning microscope (LSM510 META, Carl Zeiss, Esslingen, Germany), and each image was analyzed and saved using the ZeissLSM image Browser (Carl Zeiss).

**Statistical analysis**

Data were expressed as mean±SEM. Input/output function data of the amplitudes were analyzed via a non-repeated measures analysis of variance (ANOVA). The significance of DPOAE amplitudes was analyzed further by post hoc multiple comparison tests using the Bonferroni procedure. The statistical difference of DPOAE threshold was determined by a two-sided Mann–Whitney's *U*-test. *P*<0.05 was accepted as the level of significance.

**RESULTS**

**Distortion product otoacoustic emission**

DPOAE responses were examined during postnatal development. Non-transgenic mice started to show a measurable response of DPOAE from P12–14 followed by gradual increase of amplitude (Fig. 1A, B, C). Significant differ-

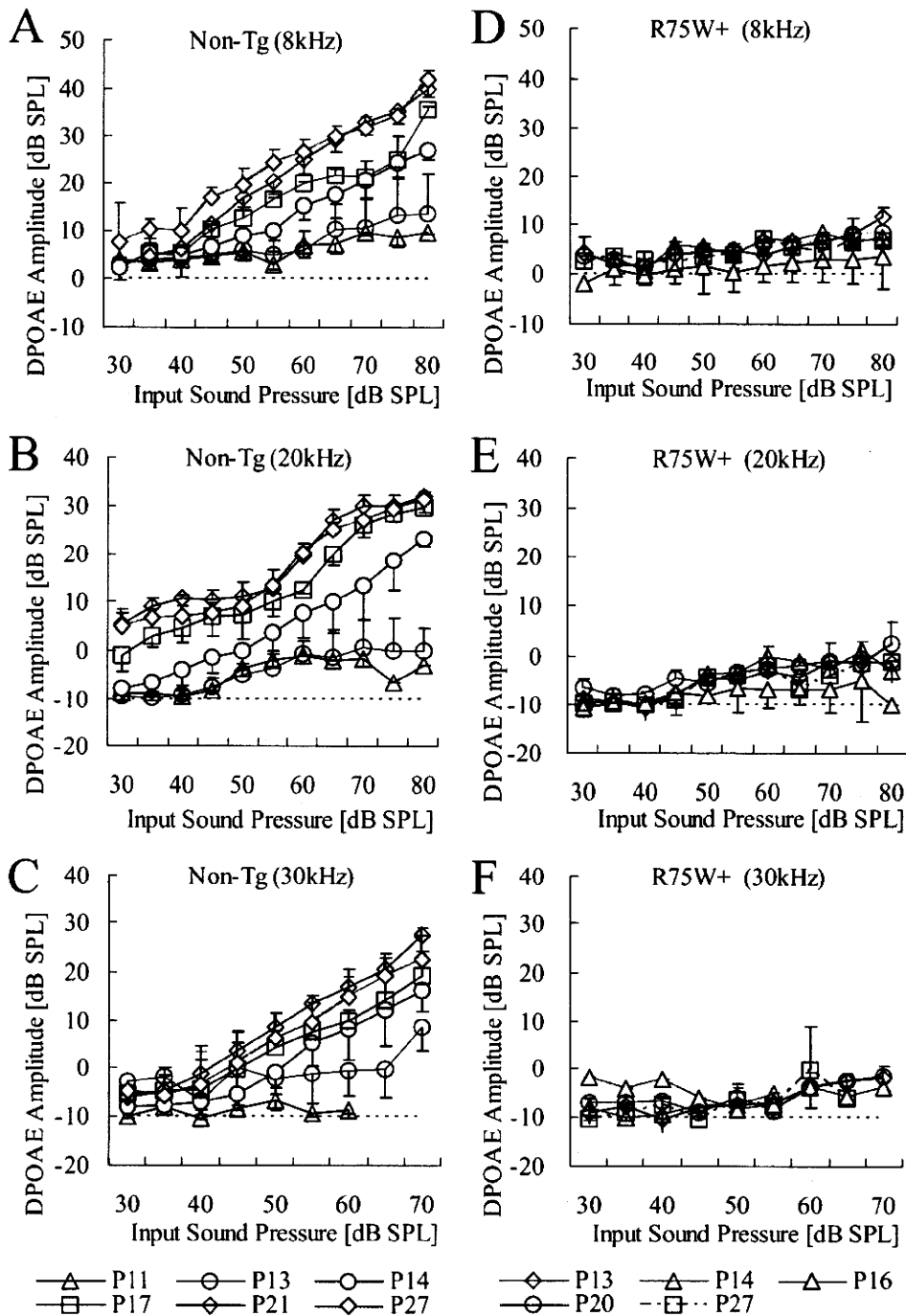


**Fig. 1.** Input/output function of the amplitudes of non-transgenic (A, B, C) and R75W transgenic (D, E, F) mice at 8 kHz, 20 kHz and 30 kHz frequencies (2f<sub>1</sub>-f<sub>2</sub>) from P11 to P27. DPOAE data were plotted as mean±SEM. The dotted line is the noise level. Non-Tg: non-transgenic mice, R75W+: R75W transgenic mice.

Please cite this article in press as: Minekawa A, et al., Cochlear outer hair cells in a dominant-negative connexin26 mutant mouse preserve non-linear capacitance in spite of impaired distortion product otoacoustic emission, *Neuroscience* (2009), doi: 10.1016/j.neuroscience.2009.08.043

ences of the DPOAE amplitudes of the non-transgenic mice in comparison to noise levels appeared at P12–14 for the different stimuli tested. In contrast, there were no statistically significant differences between noise level and DPOAE amplitudes at 8 kHz, 20 kHz, and 30 kHz throughout postnatal development in the R75W transgenic mice. Furthermore, no DPOAE was detected at any frequencies in R75W transgenic mice throughout postnatal development (Fig. 1D, E, F).

The mean DPOAE thresholds of non-transgenic mice were abruptly reduced around P13–P14 to reach the adult level by P16. In contrast, the mean DPOAE thresholds of R75W transgenic mice stayed at high level throughout postnatal development (Fig. 2).

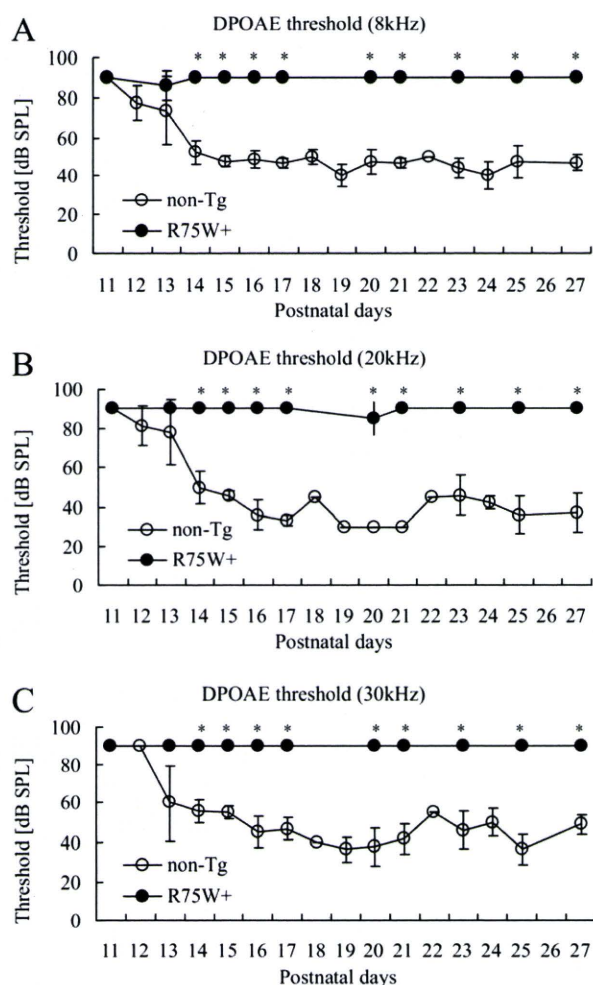


**Fig. 2.** DPOAE thresholds at 8 kHz (A), 20 kHz (B), and 30 kHz (C) frequencies of non-transgenic mice (open circle) and R75W transgenic mice (filled circle) from P11 to P27. The DPOAE threshold level was defined as the dB level at which the 2f<sub>1</sub>–f<sub>2</sub> distortion product was more than 10 dB above the noise level. In the case of no DPOAE, the threshold level was defined as 90 dB. \*: Significant difference between non-transgenic and transgenic mice ( $P < 0.05$ ). Non-Tg: non-transgenic mice, R75W+: R75W transgenic mice.

## Histology and immunohistochemistry

The cytoarchitecture of the organ of Corti of the R75W transgenic mouse was remarkably different from that of the non-transgenic mouse (Fig. 3A, B). Transverse sections of the organ of Corti in R75W transgenic mouse revealed compression and squeezing of the OHC by the surrounding supporting cells, and Nuel's space around each OHC was occupied by Deiter's cells (Fig. 3B). Structural changes in the OHCs and adjacent cells are likely to restrict the electrically-induced motility of the OHC. The mesothelial cells associated with the basilar membrane in the transgenic mouse were cuboidal and more densely packed in contrast to a flattened layer in the control mouse. However, the ultrastructure of the OHCs in the non-transgenic mouse was comparable to that of the R75W transgenic mouse (Fig. 3C, D). The OHC of both mice showed consistent characteristic features; (i) a relatively high proportion of cytoplasm having a basally located nucleus, (ii) a smooth plasma membrane lined by a thick layer of subsurface cisternae, (iii) numerous mitochondria along the lateral membrane, and (iv) no vacuole formation in the cytoplasm and no condensation of chromatin in the nucleus.

Immunofluorescence microscopy of cross-cochlear sections was used to examine the distribution of prestin in the apical turns of the cochlea of non-transgenic and R75W transgenic mice at P12. Prestin labeling was clearly visible on the whole OHC basolateral wall in both the control (Fig. 4A) and R75W+ mice (Fig. 4B) at P12. On the other hand, the nucleus and the cuticular plate of both mice were devoid of immunostaining.

These ultrastructural and immunohistochemical results support the notion that the OHC are equipped with the morphological and molecular bases to produce electromotility.

## Electromotility of OHCs

The signature electrical response of an adult OHC is a bell-shaped, voltage-dependent capacitance, which represents the conformational fluctuations of the motor molecule. In wild-type of C57BL/6J mice,  $C_v$  increased rapidly during development, saturating at P18 (Abe et al., 2007). OHCs from both R75W transgenic and non-transgenic mice showed somatic shape change in response to the voltage change (data not shown) and showed a typical bell-shaped voltage dependence (Fig. 5A).  $C_v$  increased progressively from P9 and saturated at P24. The time course of  $C_v$  in R75W transgenic and non-transgenic mice showed no significant difference (Fig. 5B). These results indicate that the development of OHC motility is not affected in R75W transgenic mice.

## DISCUSSION

The present study demonstrated that a dominant-negative R75W mutation of *Gjb2* failed to generate a detectable DPOAE from birth in spite of the presence of OHCs and apparently normal electromotility. The DPOAE depends on two factors, an intact OHC system (Long and Tubis, 1988; Brown et al., 1989) and a positive endocochlear potential

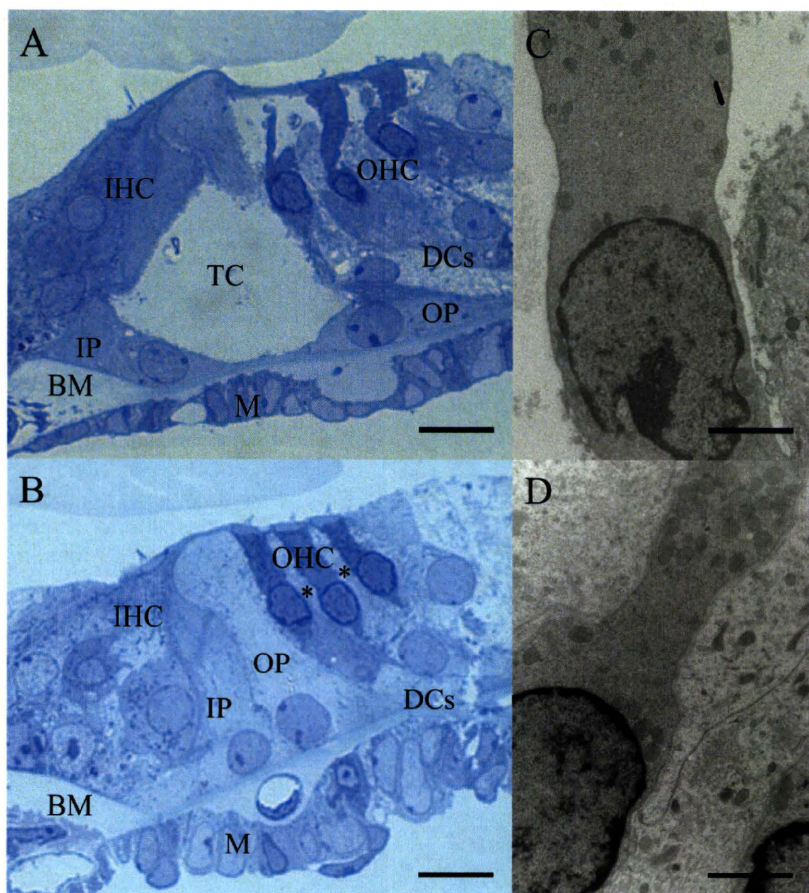


**Fig. 3.** Histology and transmission electron micrographs of non-transgenic (A, C) and R75W transgenic (B, D) mice. At P12, tunnel of Corti is detected in non-transgenic mice (A), but not (asterisk) in R75W transgenic mice (B). Nuel's space is formed in non-transgenic mice (A, C), but not in R75W transgenic mice (B, D). OHCs are detected in both non-transgenic (A) and R75W transgenic mice (B), but are squeezed by the surrounding Deiter's in R75W transgenic mice (B). The OHCs showed normal development, with preserved fine structure of the lateral wall, membrane-bound subsurface cisterna beneath the plasma membrane, and enriched mitochondria in both the non-transgenic (C) and R75W transgenic mice (D). Scale bars are 10  $\mu\text{m}$  (A, B) and 2  $\mu\text{m}$  (C, D). Abbreviations used: TC, tunnel of Corti; IP, inner pillar cell; OP, outer pillar cell; BM, basilar membrane; M, mesothelial cell.

(Brownell, 1990). The R75W transgenic mice have a normal endocochlear potential (Kudo et al., 2003). Furthermore, the OHC develops normally with apparently intact fine structure of the lateral wall, including normal membrane-bound subsurface cisterna beneath the plasma membrane. The characteristic phenotype observed in the R75W transgenic mice was the absence of the tunnel of Corti, Nuel's space, and spaces surrounding the OHC, related to abnormal development of the supporting cells.

The mammalian cochlea uses a unique mechanism for amplification of sound signals. Cochlear amplification is thought to originate from (1) somatic motility based on the cochlear motor prestin and (2) hair cell bundle motor related to mechano-electrical channel (Robles and Ruggero, 2002). Distortion and cochlear amplification are believed to stem from a common mechanism. A recent study (Verpy et al., 2008) postulated that the main source of cochlear waveform distortions is a deflection-dependent hair bundle stiffness derived from stereocilin associated with the horizontal top connectors. However, the relationship between stereocilin and prestin is still unclear.

Somatic electromotility of the OHC is a voltage-dependent rapid alteration of OHC length and stiffness. The electromotility of the OHC is thought to amplify the motion of the basilar membrane at low sound pressure levels and compress it at high levels (Patuzzi et al., 1989; Ruggero and Rich, 1991; Kossl and Russell, 1992). Prestin, which resides in the basolateral membrane of the cochlear OHC (Yu et al., 2006), acts as a voltage-dependent motor protein responsible for OHC electromotility (Belyantseva et al., 2000; Zheng et al., 2000; Liberman et al., 2002). The present study demonstrated that the voltage-dependent, nonlinear capacitance representing the conformational fluctuations of the motor molecule progressively increased from P10 to P18 in *Gjb2* R75W transgenic mice. The developmental changes in the OHC electromotility observed in the *Gjb2* R75W transgenic mice resemble those of both the C57BL/6J mouse in a previous study (Abe et al., 2007) and the littermate non-transgenic mice in the present study.

At least three factors that could explain the discrepancy between the DPOAE and the OHC electromotility

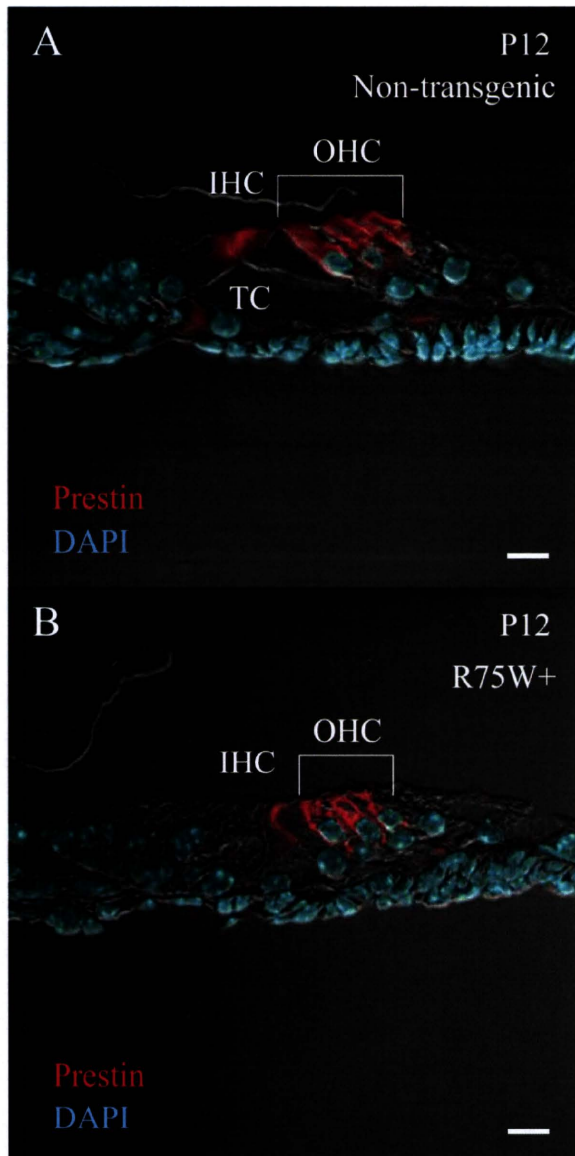


**Fig. 4.** A cross-sectional immunofluorescent analysis of prestin distributed in the apical turns of the cochlea of non-transgenic (A) and R75W transgenic mice (B) at P12. Prestin labeling (red) is clearly visible on the whole OHC basolateral wall in both the non-transgenic (A) and R75W transgenic mice (B) at P12. The extracellular space around the OHC in R75W transgenic mice is narrower than that in non-transgenic mice. On the other hand, the nucleus stained with DAPI (blue) and the cuticular plate of both mice are devoid of immunostaining. Abbreviations used: OHC, outer hair cell; IHC, inner hair cell. Scale bars are 10  $\mu\text{m}$  (A, B).

arising from the failure of development of the supporting cells can be proposed. First, mature OHCs are supported by underlying Deiter's cells, flanked on the lateral edge by a several rows of Hensen's cells, and anchored by the reticular lamina at their apical surface. The three-dimensional structure of the OHCs enable the longitudinal changes driven by transmembrane potential changes. In

the transgenic mouse, the OHCs were compressed by the surrounding Deiter's cells, thus restricting motility. Second, vibration of the basilar membrane may be related to its thickness, which would contribute to the sensitivity and the production of the otoacoustic emissions (Kossl and Vater, 1985) and further to the tonotopic changes of the developing gerbil cochlea (Schweitzer et al., 1996). The thickened basilar membrane observed in the transgenic mice might suppress the DPOAE by reducing the basilar membrane vibration. Structural changes in the basilar membrane may also reduce the sound-induced vibration of the cochlear partition, thus inhibiting deflection of stereocilia on inner hair cells. This could explain why *Gjb2* R75W transgenic mice show remarkable elevation of the auditory brainstem response threshold (Inoshita et al., 2008). Third, morphometric analysis of the organ of Corti suggest possible changes in ionic composition of the cortilymph surrounding the basolateral surface of the OHCs (Inoshita et al., 2008). Increased  $\text{K}^+$  ions in the cortilymph would de-

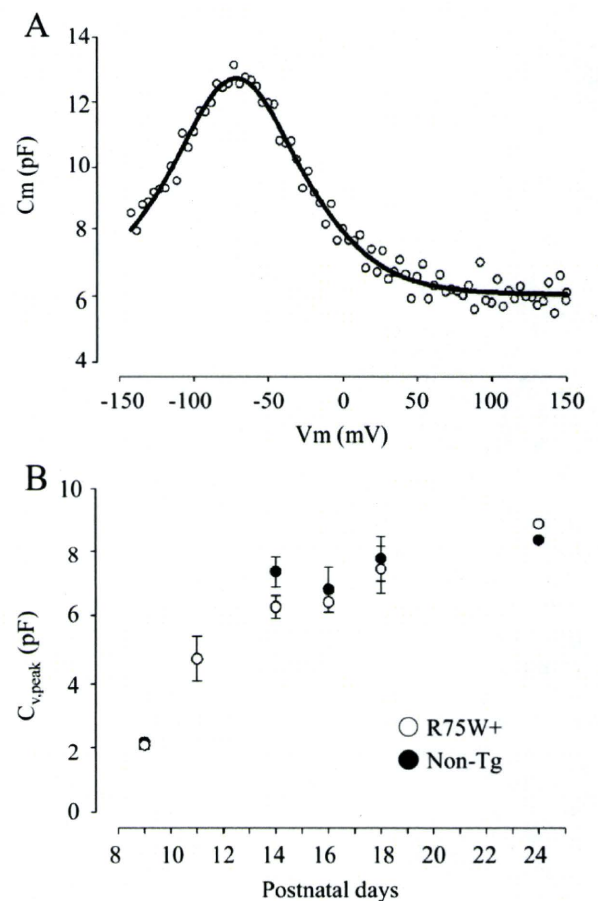


**Fig. 5.** Electrical responses of isolated OHC.  $C_m$  is expressed as a function of  $V_m$  at P14 in the R75W transgenic mouse (A). Fitted parameters are  $Q_{\text{max}}=0.704$  pC,  $z=0.89$ .  $C_{v,\text{peak}}$  is expressed as a function of postnatal day (B). The number of cells in non-transgenic (closed circle) and R75W transgenic mice (open circle) was (from P9 to P24) 1–2, 0–3, 2–3, 5–2, 3–3, and 1–1, respectively. Standard error is plotted. Non-Tg: non-transgenic mice, R75W+: R75W transgenic mice.

polarize the OHCs, and decreased driving force across the mechanosensitive channels could affect OHC electromotility. The progressive degeneration of OHCs observed in the adult R75W transgenic mice (Kudo et al., 2003) may be brought about by disturbed homeostasis of the cortilymph.

The secondary hair cell loss in adult R75W transgenic mice (Kudo et al., 2003; Inoshita et al., 2008) implies that the restoration of hearing requires the regeneration of hair cells in addition to introduction of the *Gjb2* gene. The present study clearly showed both morphological and functional maturation of OHC until late in development, suggesting that a dominant-negative R75W mutation of *Gjb2* does not affect the genes that determine or control the differentiation of the OHC. Therefore, gene transfer of *Gjb2* into the supporting cells before hair cell degeneration could be used to treat deafness. Transgene expression has been accomplished in the supporting cells of the neonatal mouse cochlea using adeno-associated viral vectors without causing additional damage to the cochlea (Iizuka et al., 2008). Therefore, the present study provides a new strategy to restore hearing in *Gjb2*-based mutation.

## CONCLUSION

OHC from the dominant-negative R75W mutation of *Gjb2* showed normal development and maturation, and isolated OHC clearly showed voltage-dependent, nonlinear capacitance with characteristic subcellular features. However, the DPOAE, which serves as an index for *in vivo* cochlear amplification, was remarkably suppressed in the mutant mice. This may result from disturbed development of the supporting cells surrounding the OHCs. The present study confirmed that the normal development of the supporting cells is indispensable for the cellular function of the OHC.

## REFERENCES

- Abe T, Kakehata S, Kitani R, Maruya S, Navaratnam D, Santos-Sacchi J, Shinkawa H (2007) Developmental expression of the outer hair cell motor prestin in the mouse. *J Membr Biol* 215:49–56.
- Beltramello M, Piazza V, Bukauskas FF, Pozzan T, Mammano F (2005) Impaired permeability to Ins(1,4,5)P<sub>3</sub> in a mutant connexin underlies recessive hereditary deafness. *Nat Cell Biol* 7: 63–69.
- Belyantseva IA, Adler HJ, Curi R, Frolenkov GI, Kachar B (2000) Expression and localization of prestin and the sugar transporter GLUT-5 during development of electromotility in cochlear outer hair cells. *J Neurosci* 20:RC116.
- Brown AM, McDowell B, Forge A (1989) Acoustic distortion products can be used to monitor the effects of chronic gentamicin treatment. *Hear Res* 42:143–156.
- Brownell WE (1990) Outer hair cell electromotility and otoacoustic emissions. *Ear Hear* 11:82–92.
- Cohen-Salmon M, Ott T, Michel V, Hardelin JP, Perfettini I, Eybalin M, Wu T, Marcus DC, Wangemann P, Willecke K, Petit C (2002) Targeted ablation of connexin26 in the inner ear epithelial gap junction network causes hearing impairment and cell death. *Curr Biol* 12:1106–1111.
- Colvin JS, Bohne BA, Harding GW, McEwen DG, Ornitz DM (1996) Skeletal overgrowth and deafness in mice lacking fibroblast growth factor receptor 3. *Nat Genet* 12:390–397.
- Forge A, Becker D, Casalotti S, Edwards J, Marziano N, Nevill G (2003) Gap junctions in the inner ear: comparison of distribution patterns in different vertebrates and assessment of connexin composition in mammals. *J Comp Neurol* 467:207–231.
- Gossman DG, Zhao HB (2008) Hemichannel-mediated inositol 1,4,5-trisphosphate (IP<sub>3</sub>) release in the cochlea: a novel mechanism of IP<sub>3</sub> intercellular signaling. *Cell Commun Adhes* 15: 305–315.
- Iizuka T, Kanzaki S, Mochizuki H, Inoshita A, Narui Y, Furukawa M, Kusunoki T, Saji M, Ogawa K, Ikeda K (2008) Noninvasive *in vivo* delivery of transgene via adeno-associated virus into supporting cells of the neonatal mouse cochlea. *Hum Gene Ther* 19:384–390.
- Inoshita A, Iizuka T, Okamura HO, Minekawa A, Kojima K, Furukawa M, Kusunoki T, Ikeda K (2008) Postnatal development of the organ of Corti in dominant-negative *Gjb2* transgenic mice. *Neuroscience* 156:1039–1047.
- Kikuchi T, Kimura RS, Paul DL, Adams JC (1995) Gap junctions in the rat cochlea: immunohistochemical and ultrastructural analysis. *Anat Embryol (Berl)* 191:101–118.
- Kitsunai Y, Yoshida N, Murakoshi M, Iida K, Kumano S, Kobayashi T, Wada H (2007) Effects of heat stress on filamentous actin and prestin of outer hair cells in mice. *Brain Res* 1177:47–58.
- Kossel M, Russell IJ (1992) The phase and magnitude of hair cell receptor potentials and frequency tuning in the guinea pig cochlea. *J Neurosci* 12:1575–1586.
- Kossel M, Vater M (1985) Evoked acoustic emissions and cochlear microphonics in the mustache bat, *Pteronotus parnellii*. *Hear Res* 19:157–170.
- Kudo T, Kure S, Ikeda K, Xia AP, Katori Y, Suzuki M, Kojima K, Ichinohe A, Suzuki Y, Aoki Y, Kobayashi T, Matsubara Y (2003) Transgenic expression of a dominant-negative connexin26 causes degeneration of the organ of Corti and non-syndromic deafness. *Hum Mol Genet* 12:995–1004.
- Liberman MC, Gao J, He DZ, Wu X, Jia S, Zuo J (2002) Pressing is required for electromotility of the outer hair cell and for the cochlear amplifier. *Nature* 419:300–304.
- Long GR, Tubis A (1988) Investigations into the nature of the association between threshold microstructure and otoacoustic emissions. *Hear Res* 36:125–138.
- Narui Y, Minekawa A, Iizuka T, Furukawa M, Kusunoki T, Koike T, Ikeda K (2009) Development of distortion product otoacoustic emissions in C57BL/6J mice. *Int J Audiol* 48:576–581.
- Patuzzi RB, Yates GK, Johnstone BM (1989) Outer hair cell receptor current and sensorineural hearing loss. *Hear Res* 42:47–72.
- Piazza V, Ciobotaru CD, Gale JE, Mammano F (2007) Purinergic signalling and intercellular Ca<sup>2+</sup> wave propagation in the organ of Corti. *Cell Calcium* 41:77–86.
- Robles L, Ruggero MA (2002) Mechanics of the mammalian cochlea. *Physiol Rev* 81:1305–1352.
- Ruggero MA, Rich NC (1991) Furosemide alters organ of Corti mechanics: evidence for feedback of outer hair cells upon the basilar membrane. *J Neurosci* 11:1057–1067.
- Santos-Sacchi J (1991) Reversible inhibition of voltage-dependent outer hair cell motility and capacitance. *J Neurosci* 11:3096–3110.
- Santos-Sacchi J (2004) Determination of cell capacitance using the exact empirical solution of partial differential Y/partial differential C<sub>m</sub> and its phase angle. *Biophys J* 87:714–727.
- Santos-Sacchi J, Kakehata S, Takahashi S (1998) Effects of membrane potential on the voltage dependence of motility-related charge in outer hair cells of the guinea-pig. *J Physiol* 510: 225–235.
- Schweitzer L, Lutz C, Hobbs M, Weaver SP (1996) Anatomical correlates of the passive properties underlying the developmental shift in the frequency map of the mammalian cochlea. *Hear Res* 97:84–94.

Please cite this article in press as: Minekawa A, et al., Cochlear outer hair cells in a dominant-negative connexin26 mutant mouse preserve non-linear capacitance in spite of impaired distortion product otoacoustic emission, *Neuroscience* (2009), doi: 10.1016/j.neuroscience.2009.08.043



- Tritsch NX, Yi E, Gale JE, Glowatzki E, Bergles DE (2007) The origin of spontaneous activity in the developing auditory system. *Nature* 450:50–55.
- Verpy E, Weil D, Leibovici M, Goodyear RJ, Hamard G, Houdon C, Lefèvre GM, Hardelin JP, Richardson GP, Avan P, Petit C (2008) Stereocilin-deficient mice reveal the origin of cochlear waveform distortions. *Nature* 456:255–258.
- Yu N, Zhu ML, Zhao HB (2006) Prestin is expressed on the whole outer hair cell basolateral surface. *Brain Res* 1095:51–58.
- Zhao HB, Yu N, Fleming CR (2005) Gap junctional hemichannel-mediated ATP release and hearing controls in the inner ear. *Proc Natl Acad Sci U S A* 102:18724–18729.
- Zhao HB, Yu N (2006) Distinct and gradient distributions of connexin26 and connexin30 in the cochlear sensory epithelium of guinea pigs. *J Comp Neurol* 499:506–518.
- Zheng J, Shen W, He DZ, Long KB, Madison LD, Dallos P (2000) Prestin is the motor protein of cochlear outer hair cells. *Nature* 405:149–155.

(Accepted 19 August 2009)

←前号に続く

### 3. Cell therapy targeting cochlear fibrocytes

神谷 和作

順天堂大学医学部耳鼻咽喉科学教室

Cell therapy targeting cochlear fibrocytes

Kazusaku Kamiya

Juntendo University School of Medicine, Department of Otoralyngology

Recently, a number of clinical studies for cell therapy have been reported and clinically used for several intractable diseases. Inner ear cell therapy for sensorineural hearing loss also has been studied using some laboratory animals, although the successful reports for the hearing recovery were still few.

Cochlear fibrocytes play important roles in normal hearing as well as in several types of sensorineural hearing loss due to inner ear homeostasis disorders. Recently, we developed a novel rat model of acute sensorineural hearing loss due to fibrocyte dysfunction induced by a mitochondrial toxin<sup>1), 2)</sup>. In this model, we demonstrate active regeneration of the cochlear fibrocytes after severe focal apoptosis without any changes in the organ of Corti. To rescue the residual hearing loss, we transplanted mesenchymal stem cells into the lateral semicircular canal; a number of these stem cells were then detected in the injured area in the lateral wall. Rats with transplanted mesenchymal stem cells in the lateral wall demonstrated a significantly higher hearing recovery ratio than controls. The mesenchymal stem cells in the lateral wall also showed connexin 26 and connexin 30 immunostaining reminiscent of gap junctions between neighboring cells<sup>3)</sup>. These results indicate that reorganization of the cochlear fibrocytes leads to hearing recovery after acute sensorineural hearing loss in this model and suggest that mesenchymal stem cell transplantation into the inner ear may be a promising therapy for patients with sensorineural hearing loss due to degeneration of cochlear fibrocytes.

---

**Key words** : cochlear fibrocyte, inner ear cell therapy, mesenchymal stem cell

**和文キーワード** : 蝸牛線維細胞, 内耳細胞療法, 間葉系幹細胞

---

Mammalian cochlear fibrocytes of the mesenchymal nonsensory regions play important roles in the cochlear physiology of hearing, including the transport of potassium ions to generate an endocochlear potential in the endolymph that is essential for the transduction of sound by hair cells<sup>4), 5), 6)</sup>. It has been postulated that a potassium recycling pathway toward the stria vascularis via fibrocytes in the cochlear lateral wall is critical for proper hearing, although the exact mechanism has not been definitively proven<sup>9)</sup>. One candidate model for this ion transport system consists of an extracellular flow of potassium ions through the scala

tympani and scala vestibuli and a transcellular flow through the organ of Corti, supporting cells, and cells of the lateral wall<sup>7), 8)</sup>. The fibrocytes within the cochlear lateral wall are divided into type I to V based on their structural features, immunostaining patterns, and general location<sup>8)</sup>. Type II, type IV, and type V fibrocytes resorb potassium ions from the surrounding perilymph and from outer sulcus cells via the Na, K-ATPase. The potassium ions are then transported to type I fibrocytes, stria basal cells and intermediate cells through gap junctions, and are secreted into the intrastrial space through potassium channels. The

secreted potassium ions are incorporated into marginal cells by the Na, K-ATPase and the Na-K-Cl cotransporter, and are finally secreted into the endolymph through potassium channels.

Degeneration and alteration of the cochlear fibrocytes have been reported to cause hearing loss without any other changes in the cochlea in the Pit-Oct-Unc (POU)-domain transcription factor Brain-4 (Brn-4) deficient mouse<sup>9</sup> and the otospiralin deficient mouse<sup>6</sup>. Brn-4 is the gene responsible for human DFN3 (Deafness 3), an X chromosome-linked nonsyndromic hearing loss. Mice deficient in Brn-4 exhibit reduced endocochlear potential and hearing loss and show severe ultrastructural alterations, including cellular atrophy and a reduction in the number of mitochondria, exclusively in spiral ligament fibrocytes<sup>9, 10</sup>. In the otospiralin deficient mouse, degeneration of type II and IV fibrocytes is the main pathological change and hair cells and the stria vascularis appear normal<sup>6</sup>. Furthermore, in mouse and gerbil models of age-related hearing loss<sup>11, 12, 13</sup>, degeneration of the cochlear fibrocytes preceded the degeneration of other types of cells within the cochlea, with notable pathological changes seen especially in type II, IV, and V fibrocytes. In humans, mutations in the connexin 26 (Cx26)

and connexin 30 (Cx30) genes, which encode gap junction proteins and are expressed in cochlear fibrocytes and non-sensory epithelial cells, are well known to be responsible for hereditary sensorineural deafness<sup>14, 15</sup>. These instances of deafness related to genetic, structural and functional alterations in the cochlear fibrocytes highlight the functional importance of these fibrocytes in maintaining normal hearing.

#### Generation of the animal model to study cochlear fibrocyte

To study the role of cochlear fibrocytes in hearing loss and hearing recovery, we developed an animal model of acute sensorineural hearing loss due to acute cochlear energy failure by administering the mitochondrial toxin 3-nitropropionic acid (3NP) into the rat round window niche<sup>1, 2</sup>. 3NP is an irreversible inhibitor of succinate dehydrogenase, a complex II enzyme of the mitochondrial electron transport chain<sup>16, 17</sup>. Systemic administration of 3NP has been used to produce selective striatal degeneration in the brain of several mammals<sup>18, 19</sup>. Our model with 3NP administration into the rat cochlea showed acute sensorineural hearing loss and revealed an initial pathological change in the fibrocytes of the lateral wall and spi-

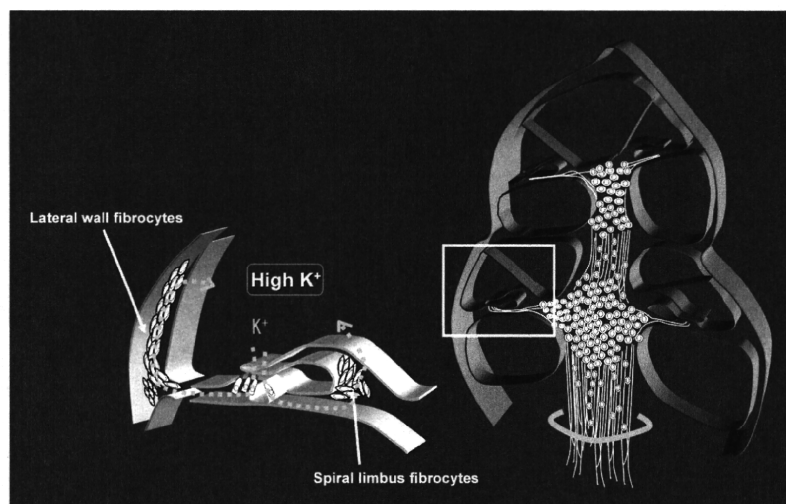


Figure. 1

The localization and the function of cochlear fibrocytes. In mammalian cochlea, ATP-dependent potassium recycling pathways have been well known as the essential mechanism for normal sound input. Cochlear fibrocytes in lateral wall and spiral limbus play a critical role in this potassium recycling system. They transport K<sup>+</sup> into the endolymph and keep high K<sup>+</sup> concentration mainly by Na<sup>+</sup>/K<sup>+</sup>-ATPase and gap junction.

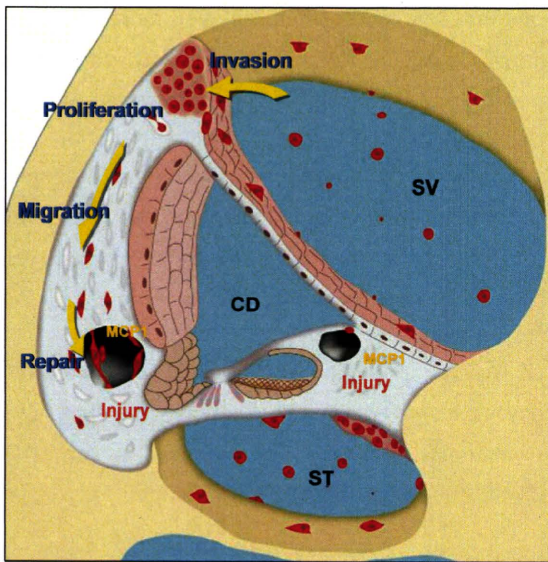


Figure. 2

A summary of the histological observations and our hypothesis for the migration of the transplanted MSCs. Arrows indicate the hypothetical route of MSC migration to the injured area. Some MSCs formed a cell mass around the scala tympani. A number of MSCs successfully invaded the lateral wall. The invading MSCs migrated and proliferated in the lateral wall. Cell migration may be induced by some chemokines such as MCP1 which was detected in our DNA microarray analysis. The MSCs which reached the injured area continued to proliferate and repaired the disconnected gap junction network. SV, scala vestibuli; CD, cochlear duct; ST, scala tympani. The schematic illustration was cited and modified from Am J Pathol, 171: 214-226, 2007 Kamiya, et al.

ral limbus without any significant damage to the organ of Corti or spiral ganglion. Furthermore, depending on the dose of 3NP used, these hearing loss model rats exhibited either a permanent threshold shift (PTS) or a temporary threshold shift (TTS). In the following study, we used doses of 3NP that induce TTS to explore the mechanism of hearing recovery after injury to the cochlear fibrocytes, and examined a novel therapeutic approach to repair the injured area using mesenchymal stem cell (MSC) transplantation.

### Mesenchymal Stem Cell (MSC) Transplantation

MSCs are multipotent cells that can be isolated from adult bone marrow and can be induced to differentiate into a variety of tissues *in vitro* and *in vivo*<sup>20</sup>. Human MSCs transplanted into fetal sheep intraperitoneally undergo site-specific differentiation into chondrocytes, adipocytes, myocytes, cardiomyocytes, bone marrow stromal cells, and thymic stroma<sup>21</sup>. Furthermore,

when MSCs were transplanted into postnatal animals, they could engraft and differentiate into several tissue-specific cell types in response to environmental cues provided by different organs<sup>22</sup>. These transplantability features of MSCs suggested the possibility that they could restore hearing loss in 3NP-treated rats to the normal range. Recently, experimental bone marrow transplantation into irradiated mice suggested that a part of spiral ligament which consists of cochlear fibrocytes was derived from bone marrow cells or hematopoietic stem cells<sup>23</sup>. This indicates that bone marrow derived stem cells such as MSC may have a capacity to repair the injury of cochlear fibrocytes.

### MSC transplantation accelerated hearing recover

The 3NP-treated rats showed complete hearing recovery at low frequencies; however, there remained a residual hearing loss at higher frequencies. Considering that the cochlear fibrocytes that were injured in this model are mesenchymal in origin, we transplanted rat MSCs into the cochlea to attempt to rescue the residual hearing loss. We used MSC which we previously established and demonstrated their potential as MSC, and we further confirmed the surface antigen expression of the cells used for transplantation in flow cytometry which showed similar expression pattern to human and murine MSCs. This suggests that the cells maintained the capacity as rat MSC at the moment of transplantation. Because there is no barrier in the inner ear perilymph between the cochlear and vestibular compartments, cells delivered from the lateral semicircular canal by perilymphatic perfusion are considered to have reached the cochlea. Within the perilymph of the cochlea, these cells presumably spread through the scala vestibuli toward the apical turn of the cochlea, and then, after passing through the helicotrema where the scala vestibuli communicates with the scala tympani, kept moving through the scala tympani toward the basal turn. There is no other way in which MSCs can spread within the cochlear perilymph.

### Invasion of MSC to lateral wall tissue

Our study clearly demonstrates that rat MSCs were

successfully transplanted into the inner ear of 3NP-treated rats by perilymphatic perfusion from the lateral semicircular canal. A number of MSCs were detected on the surface of the ampullary crest facing the perilymph and some of them were detected within the tissue of the ampullary crest, indicating that MSCs survived at least for 11 d after the perfusion and had maintained their ability to invade and migrate into the inner ear tissue. In the cochlea, a number of MSCs formed cell masses on the surface of the scala timpani, where the majority of the surrounding tissue is bone tissue, suggesting that these MSCs did not invade the cochlear tissue. In the scala vestibuli, a small number of MSCs were also found attached to the surface of the bone and the Reissner membrane. However, in the apical part of the lateral wall, a number of MSCs were observed within the tissue, suggesting that MSCs had successfully invaded the lateral wall from the perilymph. This area may be an optimum site for MSC invasion. Furthermore, we performed DNA microarray analysis of the cochlear lateral wall RNAs in 3NP-treated rats and found a significant increase in the expression of the small inducible cytokine A2 gene encoding monocyte chemoattractant protein 1 (MCP1), which has been reported as a chemokine that induces migration of neural stem cells<sup>24</sup>. This may suggest that the MSC migration to the injured area of the lateral wall in this study may also be induced by chemokines because most MSCs were observed in the lateral wall in basal turn which had a prominent damage, but not in the apical turn.

### Conclusion

Bone marrow MSCs have greater advantages for clinical use in human subjects than other multipotential stem cells, such as embryonic stem cells, because MSCs can be collected from the patient's own bone marrow for an autologous transplantation with little physical risk, no rejection risk, and few ethical problems. In the present transplantation, many MSCs were confirmed to have invaded the lateral wall and to have contributed to recovery of hearing loss despite transplantation between different rat strains. Therefore, we expect that autologous transplantation

of bone marrow MSCs would be even more effective in treating hearing loss caused by injuries to the cochlear fibrocytes. In addition, significant improvement of hearing by MSC transplantation between different rat strains indicates a possibility of allogenic transplant. Even temporary effects by allogenic transplant may cause difference in the final outcome of hearing recovery by promoting regeneration or viability of host fibrocytes during acute period of injury.

Cell therapy targeting regeneration of the cochlear fibrocytes may therefore be a powerful strategy to cure sensorineural hearing loss that cannot be reversed by current therapies.

### Acknowledgments

Most of the works had been done in National Institute of Sensory Organ, Japan (NISO). Special thanks for all the members of Laboratory of Auditory Disorders, NISO.

### References

- 1) Hoya N, et al.: A novel animal model of acute cochlear mitochondrial dysfunction. *Neuroreport*, 15: 1597-1600, 2004.
- 2) Okamoto Y, et al.: Permanent threshold shift caused by acute cochlear mitochondrial dysfunction is primarily mediated by degeneration of the lateral wall of the cochlea. *Audiol. Neurootol.*, 10: 220-233, 2005.
- 3) Kamiya K, et al.: Mesenchymal stem cell transplantation accelerates hearing recovery through the repair of injured cochlear fibrocytes. *Am J Pathol*, 171: 214-226, 2007.
- 4) Wangemann P: K<sup>+</sup> cycling and the endocochlear potential. *Hear. Res.*, 165: 1-9, 2002.
- 5) Weber PC et al.: Potassium recycling pathways in the human cochlea. *Laryngoscope*, 111: 1156-1165, 2001.
- 6) Delprat B et al.: Deafness and Cochlear Fibrocyte Alterations in Mice Deficient for the Inner Ear Protein Otospiralin. *Mol. Cell. Biol.*, 25: 847-853, 2005.
- 7) Kikuchi T, et al.: Gap junctions in the rat cochlea: immunohistochemical and ultrastructural analysis. *Anat Embryol. (Berl)*, 191: 101-118, 1995.
- 8) Spicer SS, Schulte, BA: The fine structure of spiral ligament cells relates to ion return to the stria

- and varies with place-frequency. *Hear. Res.*, 100: 80-100, 1996.
- 9) Minowa O, et al.: Altered cochlear fibrocytes in a mouse model of DFN3 nonsyndromic deafness. *Science*, 285: 1408-1411, 1999.
- 10) Xia AP et al.: Late-onset hearing loss in a mouse model of DFN3 non-syndromic deafness: morphologic and immunohistochemical analyses. *Hear. Res.*, 166: 150-158, 2002.
- 11) Spicer SS, Schulte, BA: Spiral ligament pathology in quiet-aged gerbils. *Hear. Res.*, 172: 172-185, 2002.
- 12) Hequembourg S, Liberman, MC: Spiral ligament pathology: a major aspect of age-related cochlear degeneration in C57BL/6 mice. *J. Assoc. Res. Otolaryngol.*, 2: 118-129, 2001.
- 13) Wu T, Marcus, DC: Age-related changes in cochlear endolymphatic potassium and potential in CD-1 and CBA/CaJ mice. *J. Assoc. Res. Otolaryngol.*, 4: 353-362, 2003.
- 14) Kelsell DP, et al.: Connexin 26 mutations in hereditary non-syndromic sensorineural deafness. *Nature*, 387: 80-83, 1997.
- 15) del Castillo I, et al.: A deletion involving the connexin 30 gene in nonsyndromic hearing impairment. *N. Engl. J. Med.*, 346: 243-249, 2002.
- 16) Alston TA, et al.: 3-Nitropropionate, the toxic substance of *Indigofera*, is a suicide inactivator of succinate dehydrogenase. *Proc. Natl. Acad. Sci. U S A*, 74: 3767-3771, 1977.
- 17) Coles CJ, et al.: Inactivation of succinate dehydrogenase by 3-nitropropionate. *J. Biol. Chem.*, 254: 5161-5167, 1979.
- 18) Brouillet E, et al.: Chronic mitochondrial energy impairment produces selective striatal degeneration and abnormal choreiform movements in primates. *Proc. Natl. Acad. Sci. U S A*, 92: 7105-7109, 1995.
- 19) Hamilton BF, Gould, DH: Nature and distribution of brain lesions in rats intoxicated with 3-nitropropionic acid: a type of hypoxic (energy deficient) brain damage. *Acta Neuropathol. (Berl)*, 72: 286-297, 1987.
- 20) Pittenger MF, et al.: Multilineage potential of adult human mesenchymal stem cells. *Science*, 284: 143-147, 1999.
- 21) Liechty KW, et al.: Human mesenchymal stem cells engraft and demonstrate site-specific differentiation after in utero transplantation in sheep. *Nat. Med.*, 6: 1282-1286, 2000.
- 22) Jiang Y, et al.: Pluripotency of mesenchymal stem cells derived from adult marrow. *Nature*, 418: 41-49, 2002.
- 23) Lang H, et al.: Contribution of bone marrow hematopoietic stem cells to adult mouse inner ear: mesenchymal cells and fibrocytes. *J. Comp Neurol*, 496: 187-201, 2006.
- 24) Widera D, et al.: MCP-1 induces migration of adult neural stem cells. *Eur. J. Cell Biol.*, 83: 381-387, 2004.

---

論文受付 21年 5月18日  
論文受理 21年 5月18日

別刷請求先：〒171-0021 東京都文京区本郷2丁目1-1  
順天堂大学医学部耳鼻咽喉科学教室 神谷 和作

---



Yuya Narui\*  
Akira Minekawa\*  
Takashi Iizuka\*  
Masayuki Furukawa\*  
Takeshi Kusunoki\*  
Takuji Koike<sup>§</sup>  
Katsuhisa Ikeda\*

\*Department of Otorhinolaryngology,  
Juntendo University School of  
Medicine, Tokyo, Japan

<sup>§</sup>Department of Mechanical  
Engineering and Intelligent Systems,  
The University of Electro-  
Communications, Tokyo, Japan

### Key Words

Development  
Mouse  
Distortion product otoacoustic  
emission  
Auditory brainstem response

### Abbreviations

ABR: Auditory brainstem response  
DPOE: Distortion product  
otoacoustic emission

## Development of distortion product otoacoustic emissions in C57BL/6J mice

### Abstract

Distortion product otoacoustic emissions (DPOAEs) have been used to examine the development of hearing in the rat and gerbil. However, no reports of DPOAE measurement from the onset of hearing in mice are available. Commercially-available components were assembled and adapted to provide a suitable probe microphone and sound delivery system for measuring DPOAE in developing C57BL/6J mice. Furthermore, DPOAE data were compared with the findings of the auditory brainstem response (ABR). DPOAEs were obtained at 8 kHz from 11 days after birth, 20 kHz from 12 days, and 30 kHz from 13 days. Adult-like patterns of DPOAE were obtained 21 days at 8 and 20 kHz, and 28 days at 30 kHz. On the other hand, the ABR thresholds at 12 to 36 kHz appeared between 11 and 12 days and were saturated at 14 days. Based on these data, the onset of measurable DPOAEs in the mouse were earlier than in the rat and gerbil. The maturation of DPOAE in the mouse begins at a lower frequency in the high frequency range. In addition, the ABR threshold reached maturation earlier than DPOAE.

The auditory function has been extensively studied in various mammals using several methods. The auditory brainstem response (ABR) has emerged as the most commonly used tool in the assessment of auditory function during development. The non-invasive character and simplicity of ABR recording has made it the tool of choice in this application. Another noninvasive tool used to assess auditory function is measurement of the distortion product otoacoustic emission (DPOAE) which is a type of cochlea-generated signal for evaluating the status of the outer hair cells in an intact endocochlear potential (Brownell, 1990). These acoustic signals, which can be recorded in the external ear canal, are generated within the cochlea in response to simultaneous stimulation of the same ear by two different frequency tones (Probst et al, 1991). DPOAEs are very sensitive to aging, noise exposure, and drug toxicity (Henley & Rybak, 1995; Parham, 1997; Mills & Rubel, 1994; Mills, 2003), and provide noninvasive probes for evaluating the cochlear functioning.

The DPOAE measurements have been used to examine the development of stimulus transduction along the basilar membrane in the rat and gerbil (Lenoir & Puel, 1987; Henley et al, 1990; Norton et al, 1991; Mills & Rubel, 1996). The fact that emissions provide frequency-specific information makes them

especially attractive for such investigations. DPOAEs have been found to be reliably measurable in neonatal gerbils (Mills & Rubel, 1996; Mills, 2004) and rats (Lenoir & Puel, 1987; Henley et al, 1990). Several investigators also (Li et al, 1999; Varghese et al, 2005; Inagaki et al, 2006; Noguchi et al, 2006; Zhu et al, 2007) have focused on DPOAEs in young mice, namely at 4 to 6 weeks of age. Recently, the mouse has been used as an animal model for various hearing disorders. It is useful to measure auditory function throughout the life of the mouse in studies such as those directed toward genetic disorders (for example, see Minowa et al, 1999; Kudo et al, 2003). However, postnatal development of DPOAEs from the onset of hearing in mice has not been reported.

A mouse is smaller than a gerbil, so it possesses a narrower external auditory canal than a gerbil and extremely high frequency hearing. Namely, in the measurement of high frequency sound, the wavelength is too short to avoid the resonance of both the external auditory meatus and the inner space of the conventional probe used for DPOAE measurements. Resonance prevents the correct measurement of the sound pressure in front of the tympanic membrane. This is one reason why there have been few reports on high frequency DPOAE measurements in neonatal rodents, other than that of Mills and Rubel (1996).



They improved the probe for gerbils, in which the internal diameter was reduced to 1.4–2.0 mm, and the speaker tube was connected to the two inlets for sound stimulus delivery.

In the present study, commercially-available transducers were adapted to provide a probe sound system for more efficacious measurement of DPOAEs during the early developmental stages of the mouse. Furthermore, the development of the DPOAE and ABR were compared during the postnatal period.

## Methods

### *Design of the probe for measurement of DPOAEs, and evaluation of the probe by using the external auditory canal model*

It was essential to adapt commercially available transducers to construct a probe system more suitable to the purposes of this study, as illustrated in Figure 1. The probe consisted of two speakers (ES1, Tucker-Davis Technologies, Alachua, FL, USA), a microphone (ER-10B+, Etymotic Research, Elk Grove Village, IL, USA), coupler tube, and plastic tip. Conical shaped couplers were attached to the speakers, and a coupler tube was connected to the conical shaped couplers. The other end of the coupler tube was inserted into the probe and then it was slightly extended to the outside of the tip of the probe. The specifications of the speaker given by the manufacturer are as follows: The typical output of the speaker is 95 dB SPL at a distance of 10 cm when a 5-kHz signal with voltage of  $\pm 9.9$  V is applied to the speaker. Although there is a dull peak at 40 kHz, the frequency response of the speaker is roughly flat from 4 kHz to 110 kHz (the variance is  $\pm 11$  dB) when a constant input voltage is applied to the speaker. Although the manufacturer has not tested the frequency response of the microphone at frequencies higher than 10 kHz, the sensitivities were previously checked by comparing the output from the reference microphone (MI1531, Ono Sokki, Tokyo, Japan), the available frequency of which was up to 100 kHz. The tip of the DPOAE probe was thinned to fit into the external auditory meatus of the neonatal mice.

When the probe was inserted into the mouse's external auditory meatus, there was a distance of about 1.5 mm between the diaphragm of the microphone of the probe and the eardrum,

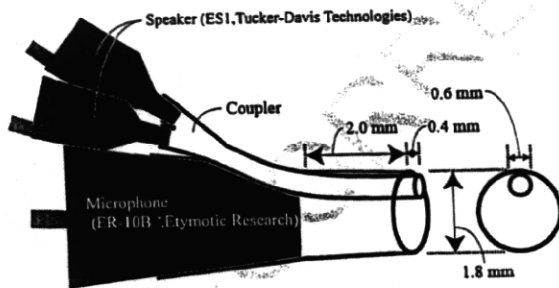


**Figure 1.** Structure of a newly developed probe. The material is plastic. The speaker tubes are used as a coupler. The end of the speaker tube is slightly extended to the outside of the tip of the probe. The microphone (model ER-10B, Etymotic Research Inc., Elk Grove Village, IL, USA) can be temporarily removed from the probe.

so that the sound pressure level detected by the microphone was different from that at the eardrum. Therefore, not only the frequency characteristics of the speakers but also that of the microphone were evaluated using an external auditory meatus model that is a plastic cylinder with 2.4 mm outside diameter, 2.0 mm inside diameter, which was determined by referring to the shape of the external auditory meatus of 12- to 14-day-old mice (Sauders & Cruemling, 2001; Sauders & Garfinkle, 1983). Figure 2 shows the experimental set up for evaluating the characteristics of the probe.

The probe was inserted into one side of the external auditory meatus model and the reference microphone was inserted into the other side, which corresponded to the eardrum. The voltage of the function generator was fixed at 12 V<sub>p-p</sub> and frequencies were swept from 1 kHz to 50 kHz. The sound pressure emitted from the speaker was simultaneously detected by the microphone of the probe and the reference microphone. The signals from the microphones were transformed into sound pressure levels using the fast Fourier transform on a personal computer using an original program. The sound pressure levels originating from the microphone of the probe and the reference microphones were compared. The examination was performed within an acoustically and electrically insulated and grounded test room.

The sound pressure detected by the microphone of the probe was almost the same as that detected by the reference microphone (Figure 3), although some differences appeared at the frequencies of 5, 6, 7, and 17 kHz. This result suggests that the probe can measure the correct sound pressure level in the external auditory meatus, i.e. in front of the tympanic membrane, and then can apply any sound pressure to the tympanic membrane by monitoring the output from the probe microphone.

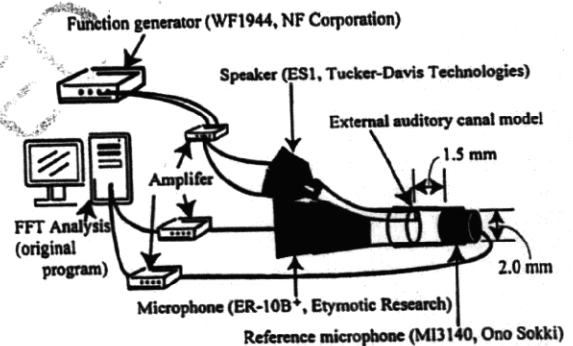


**Figure 2.** Experimental set up for evaluating the characteristics of the probe using the external auditory canal model. The microphone (ER-10B, Etymotic Research Inc., Elk Grove Village, IL, USA) and speakers (ES1, Tucker-Davis Technologies, Alachua, FL, USA) are set into the newly developed probe, and the probe and the reference microphone (MI3140, Ono Sokki, Yokohama, Japan) are connected to both sides of the external canal model with 2.4 mm outside diameter and 2.0 mm inside diameter. The speakers are connected to a function generator (WF1944, NF Corporation, Yokohama, Japan) through the amplifiers, and the microphones are connected to a fast Fourier transform (FFT) analyser (FFT is performed on a personal computer using an original program) through the different amplifiers.

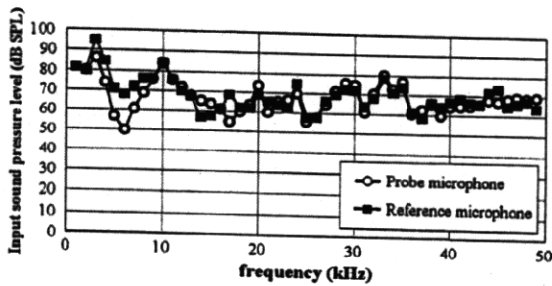


**Figure 3.** The measurement of sound pressure in an external ear canal model. Sound pressure levels are detected by the microphone of the probe and the reference microphone corresponding to the eardrum. Each dot represents the time ensemble averages of 256 epochs. The voltage of the function generator is fixed at 12 Vp-p and frequencies are swept from 1 kHz to 50 kHz. The differences greater than 10 dB between these microphones appeared at constant frequency areas such as 5, 6, 7, and 17 kHz.

#### Animals

C57BL/6J mice were purchased from a commercial breeder (CLEA Japan Inc., Tokyo, Japan). The range of ages was 9–28 days after birth. The mice were housed in temperature-controlled rooms at the vivarium in polyurethane cages bedded with wood chips. Free access to food and water was provided. The cages were cleaned twice weekly. At the beginning of each data-collection session, the mice were lightly anesthetized with an initial intramuscular dose of ketamine hydrochloride (100 mg/kg) and xylazine hydrochloride (4 mg/kg). Anesthesia was maintained by administering additional, less concentrated doses (ketamine, 50 mg/kg; xylazine, 2 mg/kg) when twitching of the vibrissae became noticeable. At all recording sessions, the body temperature was maintained near 37°C with a heating pad. The care and study protocol were approved by the Animal Care Committee at Juntendo University School of Medicine.

#### DPOAE recording systems and procedures

The newly developed probe was inserted into the left ear after examination for signs of middle ear infections or unusual buildup of cerumen in the ear canal. Animals that experienced either death or signs of middle-ear problems in the course of experiments were excluded from the study, so the final numbers of ears that yielded functional data were: nine days after birth,  $n=3$ ; 10 days after birth,  $n=3$ ; 11 days after birth,  $n=5$ ; 12 days after birth,  $n=5$ ; 13 days after birth,  $n=4$ ; 14 days after birth,  $n=3$ ; 15 days after birth,  $n=5$ ; 16 days after birth,  $n=4$ ; 17 days after birth, 21 days after birth,  $n=4$ , and 28 days after birth,  $n=4$ . When inserting the probe into the external auditory meatus, a small incision was made if necessary.

DPOAE stimuli consisted of two primary frequencies,  $f_1$  and  $f_2$ , such that  $f_1 < f_2$ . DPOAE input/output functions at  $f_2 = 12, 30,$  and  $45$  kHz with  $f_2/f_1 = 1.2$  were constructed. At each frequency pair, primary levels L1 (level of  $f_1$  tone) and L2 (level of  $f_2$  tone) were incremented in 5 dB steps from 20 to 80 dB ( $f_2 = 12$  kHz), 20 to 75 dB ( $f_2 = 30$  kHz), and 20 to 70 dB ( $f_2 = 45$  kHz) with  $L_1 = L_2$  (Parham et al, 2001).

#### ABR recording system and procedures

Five mice were anesthetized within an acoustically and electrically insulated and grounded test room. The stainless-steel needle electrodes were placed at the bregma (active), the retroauricular region (inactive), and abdomen (ground). The acoustic stimuli were synthesized and produced using TDT System 3 and delivered to the mice through a speaker (ES1 with the conical shaped coupler, which is the same as that used for DPOAE measurements, but without the coupler tubes). The calibration of the sound intensity generated by the speaker was done by measuring the sound pressure near the outlet of the speaker with a precision integrating sound level meter (LA5111, ONO SOKKI). Pure-tone bursts (0.5 ms rise/fall time, 2 ms duration, 200 ms repetition period, 128 repetitions) were delivered in 5-dB steps between 0 and 85 dB sound pressure level at 12, 24, and 36 kHz. The electrodes were connected to an extra cellular amplifier AC PreAmplifier (model P-55, Astro-Med, West Warwick, RI, USA), and ABR waveforms were analysed using the PowerLab system software program (model PowerLab4/25, AD Instruments, Castle Hill, Australia). The lowest stimulus level that yielded a detectable wave I of ABR was defined as the threshold. If the hearing threshold was over 85 dB, then it was assigned a value of 90 dB.

#### Statistics

Data were expressed as the mean  $\pm$  SEM and analysed via a non-repeated measures analysis of variance (ANOVA). Significant effects were analysed further by post hoc multiple comparison tests using the Bonferroni and Student-Newman-Keuls procedure.

#### Results

##### Distortion product otoacoustic emissions in neonatal C57BL/6J mice

The developmental trends for the mean input/output (I/O) functions of 2 $f_1$ - $f_2$  DPOAEs at 8, 20, and 30 kHz including the mean noise floors across the test frequencies are presented in Figure 4. No DPOAE responses could be elicited before 11 days after birth. The DPOAEs at 65 dB of input sound pressure could be significantly detected at 8 kHz from 11 days after birth, 20 kHz from 12 days after birth and the 30 kHz from 13 days after birth (Table 1). As development progressed, the range of the primary levels required to register DPOAEs decreased to low values, and the maximum level of the response quickly increased. The DPOAE at 65 dB of input sound pressure reached a plateau at 21 days after birth at 8 and 20 kHz. However, at 30 kHz, DPOAE amplitude 21 days after birth was slightly but significantly different from that of 28 days after birth ( $P < 0.05$ ; Table 1).

##### Auditory brainstem responses in neonatal C57BL/6J mice

As illustrated in Figure 5, wave I of the ABR elicited by a tone burst was not detected until 10 days after birth. The wave I of ABR was significantly detected 11 days after birth at 12 and 24 kHz, and 12 days after birth at 36 kHz. The ABR thresholds were gradually reduced and saturated 14 days after birth at all tested frequencies.

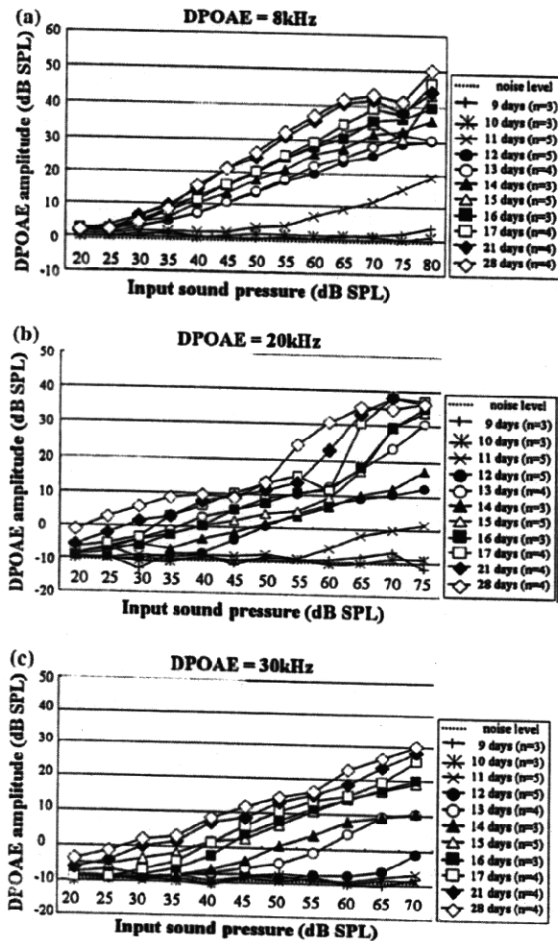


**Figure 4.** The developmental trends for the mean input/output functions of 2f<sub>1</sub>-f<sub>2</sub> DPOAEs at 8 (a), 20 (b), and 30 kHz (c). Note the mean noise floors from individual mice of different ages. The level of these responses is expressed as input sound pressure levels. DPOAEs are obtained at 8 and 20 kHz from 11 days and older mice, whereas the 13-day-old mice first respond to 30 kHz.

## Discussion

### Improvement of the probe

Some slight modifications were applied to the conventional probe microphone systems as described by Mills and Rubel (1996) to the study of mice, such as reducing the diameter of the probe and use two inlets for sound-stimulus delivery to the additional improvement. The microphone was temporarily removed from the hole of the probe for visualizing the external ear canal through the hole. Furthermore, the probe was thinned to fit into the external auditory meatus of the neonatal mice. However, when the probe tip was thinned, a small cavity with a narrow outlet was formed in the probe. In this case, if the stimulus sound was emitted into the cavity in the probe, only the sound pressure in the cavity increases, and the stimulus sound cannot be emitted to the outside of the probe. To avoid such a resonance of the probe and

to emit sounds to the eardrum efficiently, the end of the coupler tube was slightly extended to outside of the tip of the probe. These developments reduced insertion time and solved the problems that occurred by reducing the diameter of the probe.

Referring to the frequency response of the speaker with a coupler tube measured and presented by the manufacturer (Tucker-Davis Technologies), no significant peaks were found in the frequency response, and the frequency response that was measured as shown in Figure 3 was similar to that presented by the manufacturer, although the speakers were connected to the probe with coupler tubes which were longer than the wavelength of the applied sounds of high frequencies. The resonance may have been avoided at high frequencies because of the damping of the tube connected to the speaker. The frequency response in Figure 3 was caused by the characteristics of the speaker itself, and both the structure of the probe and the model of the external auditory canal scarcely affected the frequency response. In addition, because the length of the model of the external auditory canal was only 1.5 mm, the standing wave may not have been generated in the canal. In contrast, since the distance between the tympanic membrane and the diaphragm of the microphone installed in the ER-10B+ was approximately 15 mm, there was a possibility that this distance caused standing waves. However, Figure 3 shows that sound pressure level detected by the microphone of the probe was almost consistent with that in front of the tympanic membrane. This point is essential to apply the proper sound pressure to the tympanic membrane and measure the sound pressure level of the DPOAEs emitted from the tympanic membrane.

### Comparison of postnatal development of DPOAEs between the mouse and other animals

The present report is the first demonstration showing the postnatal development of DPOAE in mice although this has been demonstrated in other rodents such as the rat and gerbil (Lenoir & Puel, 1987; Henley et al, 1989; Norton et al, 1991; Mills et al, 1993; Mills & Rubel, 1996). A significant DPOAE response could be obtained at 8 kHz from 11 days after birth, 20 kHz from 12 days, and 30 kHz from 13 days after birth, 20 kHz from 21 days after birth at 8 and 20 kHz, and 28 days after birth at 30 kHz. Investigation of the cochlear function at the onset of auditory responses has been performed by measuring DPOAE in the rat and gerbil (Lenoir & Puel, 1987; Henley et al, 1989; Norton et al, 1991; Mills et al, 1993; Mills & Rubel, 1996). In both rodent species, all reports indicated that DPOAEs were detected first 12–14 days after birth, which is later than that of the mice investigated in the present study. In mammals, DPOAE develops in a frequency-specific fashion. In low frequency ranges, Lenoir and Puel (1987) reported that maturation of the DPOAEs was found first at a high frequency in rat pups (measurement of DPOAEs to 2f<sub>1</sub>-f<sub>2</sub> = 3, 5, and 7 kHz). Henley (1990) reported similar data suggesting that responses were first detected from a high frequency in rat pups (measurement of DPOAEs to 2f<sub>1</sub>-f<sub>2</sub> = 2.8–8.0 kHz). Norton et al (1991) detected responses first from a high frequency (measurement of DPOAEs 2f<sub>1</sub>-f<sub>2</sub> = 1.3–13.0 kHz) in gerbils. Mills and Rubel (1996) reported that maturation begins first at a lower frequency in the high frequency range (measurement of DPOAEs to 2f<sub>1</sub>-f<sub>2</sub> = 0.5–48 kHz), which was consistent with the current findings that maturation of DPOAE began first at a lower frequency in the high frequency

**Table 1.** Comparison of DPOAE amplitudes (mean  $\pm$  S.E.) among postnatal days at 8, 20, and 30 kHz (input sound pressure = 65 dB).

Noise level	Amplitude (dB SPL)	noise level	P9	P10	P11	P12	P13	P14	P21	P28
8 kHz	0									
P9	0.98 $\pm$ 0.03		n.s.	n.s.	P < 0.05	P < 0.01	P < 0.01	P < 0.01	P < 0.01	P < 0.01
P10	1.2 $\pm$ 0.18			n.s.	P < 0.01	P < 0.01	P < 0.01	P < 0.01	P < 0.01	P < 0.01
P11	8.48 $\pm$ 2.53				P < 0.01	P < 0.01	P < 0.01	P < 0.01	P < 0.01	P < 0.01
P12	23.57 $\pm$ 4.41					P < 0.01	P < 0.01	P < 0.01	P < 0.01	P < 0.01
P13	25.06 $\pm$ 3.06						n.s.	n.s.	P < 0.01	P < 0.01
P14	27.67 $\pm$ 1.45							n.s.	P < 0.01	P < 0.01
P21	40.56 $\pm$ 0.65								P < 0.01	P < 0.01
P28	41.73 $\pm$ 0.65									n.s.
20 kHz	-10									
P9	-8.29 $\pm$ 0.84		n.s.	n.s.	n.s.	P < 0.01	P < 0.01	P < 0.01	P < 0.01	P < 0.01
P10	-10.28 $\pm$ 0.67			n.s.	n.s.	P < 0.01	P < 0.01	P < 0.01	P < 0.01	P < 0.01
P11	-1.94 $\pm$ 0.12				P < 0.01	P < 0.01	P < 0.01	P < 0.01	P < 0.01	P < 0.01
P12	9.03 $\pm$ 2.18					P < 0.01	P < 0.01	P < 0.01	P < 0.01	P < 0.01
P13	15.66 $\pm$ 2.20						P < 0.01	n.s.	P < 0.01	P < 0.01
P14	13.67 $\pm$ 3.53							n.s.	P < 0.01	P < 0.01
P21	33.21 $\pm$ 3.17								P < 0.01	P < 0.01
P28	34.90 $\pm$ 2.23									n.s.
30 kHz	-10									
P9	-10.16 $\pm$ 1.03		n.s.	n.s.	n.s.	n.s.	P < 0.01	P < 0.01	P < 0.01	P < 0.01
P10	-8.41 $\pm$ 0.60			n.s.	n.s.	n.s.	P < 0.01	P < 0.01	P < 0.01	P < 0.01
P11	-7.77 $\pm$ 1.78				n.s.	n.s.	P < 0.01	P < 0.01	P < 0.01	P < 0.01
P12	-6.17 $\pm$ 2.66					n.s.	P < 0.01	P < 0.01	P < 0.01	P < 0.01
P13	9.29 $\pm$ 4.28						P < 0.01	P < 0.01	P < 0.01	P < 0.01
P14	9.29 $\pm$ 0.99							n.s.	P < 0.01	P < 0.01
P21	23.66 $\pm$ 1.52								P < 0.01	P < 0.01
P28	28.64 $\pm$ 0.83									P < 0.05

n.s. = not significant.

range (at 8 and 20 kHz). The available data in mammals indicate that the representation of low frequencies at the cochlear apex is developmentally stable, whereas the tonotopy shifts at more basal (mid- and high-frequency) locations. This model of the development of peripheral tonotopy is likely to be explained by developmental changes in the passive mechanical properties of the basilar membrane and the active cochlear process (Norton et al, 1991; Mills & Rubel, 1996), but this bears further examination.

#### Differences between DPOAE and ABR during development

In the present study, the mice showed a discrepancy in maturation between the DPOAE amplitude and ABR threshold. No studies have investigated the relationship between DPOAE and ABR in the postnatal period of the mammalian cochlea. The DPOAE amplitude in the mouse showed a saturating increase from 11 to 20 days, which reached a plateau at 21 to 28 days after birth. Abe et al (2007) reported that nonlinear capacitance (observed using the isolated outer hair cell of mice) increases until 18 days after birth, which is somewhat consistent with the DPOAE maturation observed in the present study. The DPOAE development corresponds to that of the outer hair cell electromotility (Long & Tubis, 1988; Brown et al, 1989). Therefore, the postnatal changes of DPOAE can be used to assess

outer hair cell functioning, contributing to frequency selectivity (tuning). On the other hand, ABR thresholds in the present study, showing detection at 11–12 days and maturation up to 14 days after birth, is comparable to trends previously reported by

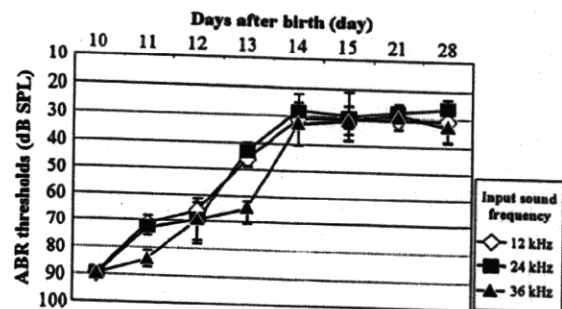


**Figure 5.** Developmental changes of ABR thresholds at 12, 24, and 36 kHz from 10 to 28 days after birth. The level of thresholds is expressed as the days after birth. The ABRs are detected first 11 days after birth at 12 and 24 kHz, and 12 days after birth at 36 kHz. The ABR thresholds are gradually reduced and saturated 14 days after birth.